Int. J. Multiphase Flow Vol. 15, No. 3, pp. 447–457, 1989
Printed in Great Britain.

0301-9322/89 $3.00 + 0.00

AN EXPERIMENTAL INVESTIGATION OF PHASE DISTRIBUTION IN AN ECCENTRIC ANNULUS

R. T. LAHEY JR and K. OHKAWA†
Department of Nuclear Engineering and Engineering Physics, Rensselaer Polytechnic Institute, Troy, NY 12180-3590, U.S.A.

(*Received* 10 *October* 1988; *in revised form* 25 *January* 1989)

Abstract—A novel new nonintrusive measurement technique, based on γ-ray scattering, has been developed and applied. In particular, the local void fraction distribution has been measured for various air/water two-phase flow regimes in an eccentric annulus. A significant amount of lateral phase distribution was observed. Indeed, the gas was found to preferentially collect in the region of the test section having the largest gap. These data trends are in agreement with prior data taken with boiling fluid, and indicate that the lateral "void drift" forces are quite strong.

Key Words: phase distribution, γ-ray densitometry, lateral "void drift", two-phase density distribution, eccentric annulus

INTRODUCTION

Multiphase flows are prevalent in many applications in the power, process and petrochemical industries. To date, however, our ability to perform mechanistic thermal-hydraulic evaluations of multiphase systems is limited by an inadequate understanding of lateral phase distribution phenomena. In particular, to accurately predict two-phase pressure drop and heat transfer one must be able to model multidimensional phase distribution.

Previous studies (Wang *et al.* 1987) have shown that turbulence-induced lateral forces are responsible for the observed phase distribution for bubbly flows in simple geometry conduits (i.e. in a vertical pipe). In contrast, our understanding of phase distribution mechanisms for various flow regimes in complex geometry conduits is not well-developed. The purpose of the experimental study presented herein was to provide information on phase distribution in eccentric annuli.

DISCUSSION

It has been known for some time (Kondic & Hahn 1970) that γ-ray scattering density measurement techniques can, in principle, be used to nonintrusively measure the local density of a two-phase system.

This type of technique was previously used to measure the density in the central subchannel of a simulated 4×4 rod fuel bundle (Zielka & MacKinnon 1977). However, in order to use the technique, the assumption was required that the density profile be azimuthally symmetric.

Other developments in γ-ray scattering measurement techniques have relied heavily on the energy dependence of Compton scattering. Elias & Ben-Haim (1980) developed an experimental procedure using a combination of a tightly-collimated initial beam and a photon detector with a wide-angle collimator. Kondic *et al.* (1983) have shown the possibility of utilizing a fan beam and a wide-angle photon detector. These methods rely on the ability to discriminate multiple-scattered photons and the one-to-one correspondence between the angle of scattering and the energy of scattered photons. While such wide-angle methods have possibilities, they do not appear to be well-suited for measurements in complex geometries (e.g. an annular test section or rod bundle) due to the presence of high-density structural materials. In addition, due to the limited resolution of most photon

† Present address; Nuclear Fuels Division, Westinghouse Electric Corp., P.O. Box 3912, MMOB, Mail Stop 4-06, Pittsburgh, PA 15230, U.S.A.

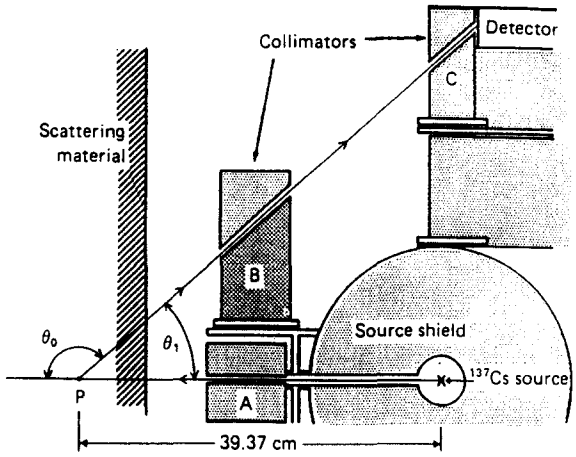

Figure 1. γ-Ray scattering densitometer.

detection systems, it is very difficult to accurately determine the location of the photon scattering site and thus the local density.

Nevertheless, nonintrusive γ-ray scattering techniques clearly possess important advantages over traditional intrusive two-phase flow measurement techniques, which disturb the flow field being measured and affect the accuracy of the measurement.

Previous γ-ray scattering techniques that were applied to the measurement of two-phase flows were based on the unrealistic assumption of ideal photon beam collimation and/or point scattering. Such models ignored the fact that the primary photon beam diverges and is attenuated within the scattering volume.

A novel new measurment device has been developed for the nonintrusive measurement of the local void fraction distribution in conduits of complex geometry (Ohkawa & Lahey 1983). The analysis of this device is based on the principle of Compton scattering of photons and does not make unrealistic assumptions concerning collimation and scattering.

Let us now consider the mathematical modeling of scattering events and detector response as a function of scattering volume position and the local density of the material in which the scattering takes place.

Figure 1 gives a schematic view of the γ-ray scattering densitometer, showing an NaI detector, three lead collimators (A, B and C), a shielded source and a scattering point, P, in the scattering material.

Scattering events occur in the following sequence. First, γ-rays (i.e. photons) with an energy of 0.662 MeV leave the ^{137}Cs source isotropically. The shield and collimator A allow photons only in the direction of P, thus giving a beam of photons that is essentially uniform in energy and direction. Upon entering the scattering material, the photon beam is attenuated by absorption and scattering. In this energy range (0.662 MeV), Compton scattering dominates over other photon interactions. Most of the photons that reach point P travel through it without interaction, while some undergo scattering or absorption. Some of the photons scattered at P eventually reach the NaI detector through two collimators, B and C. As the densitometer (which includes the source, the collimators and the dectector) moves relative to the scattering material, the detector response changes, reflecting the local density at point P and beam attenuation up to, and from, point P. Let us now review the Compton scattering theory on which the γ-ray scattering densitometer is based.

A photon has its energy reduced when scattered by an electron. Its resulting energy can be calculated as

$$E_1 = \frac{E_e}{\left(1 - \cos\theta + \frac{E_e}{E_0}\right)} \qquad [1]$$

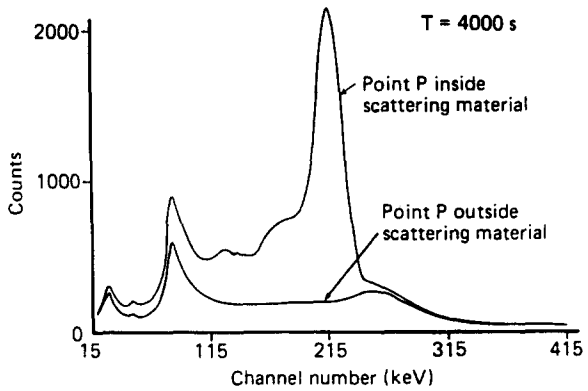

Figure 2. Energy distribution of photons reaching the detector.

and its differential cross section is given by the well-known Klein–Nishina formula (Knoll 1979):

$$\frac{d\sigma_{c(\theta)}}{d\Omega} = 0.023\frac{Z}{A}\eta^2(\eta^{-1} + \eta - \sin^2\theta) \qquad \text{cm}^2/\text{g sr}, \qquad [2]$$

where

Z/A = number of electrons per atom of the mixture,
$\eta = E_1/E_0$,
E_0 = initial energy (MeV),
E_1 = energy of the scattered photon (MeV),
$E_e = 0.511$ MeV, the rest mass energy of an electron,

and

θ = scattering angle.

A typical measured counts vs energy response, when P is inside and outside the scattering material, is shown in figure 2. The peak at 0.202 MeV is due to photons that are scattered through an angle θ, from the scattering point P, and have reached the detector through the two collimators (B and C). Since, as described by [1], single-scattered photons are uniquely related to the scattering angle, one can determine the response from point P by setting the window of a single-channel analyzer on the 0.202 MeV peak. Unfortunately, this does not eliminate the effect of multiple scattering (Ohkawa & Lahey 1983). This poses a potentially serious problem since it implies that photons may be counted even after experiencing two or more collisions. Thus, the detector response function, $D(Z)$, consists of four components:

$$D(Z) = C^{(1)}(Z) + C^{(m)}(Z) + B + e(Z), \qquad [3]$$

where

$D(Z)$ = detector response (i.e. the counting rate),
$C^{(1)}(Z)$ = counting rate due to single-scattered photons,
$C^{(m)}(Z)$ = counting rate due to multiple-scattered photons,
B = background

and

$e(Z)$ = measurement noise.

Each component can be derived either theoretically or experimentally, as will be discussed.

Let us first consider single-scattered photons. Assume the source is at the origin and the source, the detector and the scattering point, P, are in the vertical plane. Let a superscript * on Z designate the distance measured from the origin, while Z without the superscript is measured from the surface of the test section.

The following are assumptions made in the derivation of the detector response for point scattering:

(1) The unattenuated γ-ray flux is a function of Z_P^* only (i.e. there is no X–Y dependence).
(2) All material properties are only functions of distance from the surface of the test section.
(3) The angle θ_1 between the incoming and outgoing photon beams stays constant within the scattering volume.
(4) Photons suffer no scattering or absorption in air.

The expression of the counting rate per unit volume from P, a point inside the scattering material, can be constructed using the well-known point kernel method (Ohkawa & Lahey 1983):

$$C_P^{(1)}(Z_P^*, Z_\dagger^*) = \epsilon_d \Phi(Z_P^*)\, \Delta\Omega(Z_P^*) \frac{d\sigma_c}{d\Omega}(Z_P^* - Z_\dagger^*) \rho(Z_P^* - Z_\dagger^*) \times \exp\left[-\int_{Z_\dagger^*}^{Z_P^*} \rho(Z' - Z_\dagger^*) \left[\frac{\mu}{\rho}\right]^{in} (Z' - Z_\dagger^*)\, dZ' \right] \times \exp\left[-\int_{Z_\dagger^*}^{Z_P^*} \rho(Z' - Z_\dagger^*) \left[\frac{\mu}{\rho}\right]^{out} (Z' - Z_\dagger^*) \frac{dZ'}{\cos\theta_1} \right], \quad [4]$$

where

ϵ_d = efficiency of the detection system,
$\Phi(Z_P^*)$ = unattenuated γ-ray flux at point P,
$C_P^{(1)}(Z_P^*, Z_\dagger^*)$ = counting rate per unit volume due to single-scattered photons from point P,
$\Delta\Omega(Z_P^*)$ = solid angle of the detector opening viewed from point P,
$\frac{d\sigma_c}{d\Omega}(Z_P^* - Z_\dagger^*)$ = differential Compton scattering cross section, which is a function of distance from the surface of the test section,
$\rho(Z_P^* - Z_\dagger^*)$ = local density, which is a function of distance from the surface of the test section,
$\left[\frac{\mu}{\rho}\right]^{in}(Z' - Z_\dagger^*)$ = mass attenuation coefficient of the scattering material for the energy of the incoming photons, which is a function of the distance from the surface of the test section,

and

$\left[\frac{\mu}{\rho}\right]^{out}(Z' - Z_\dagger^*)$ = mass attenuation coefficient of the material for the energy of the scattered (at angle θ_1) photons, which is a function of the distance from the surface of the test section.

The last two exponential terms in [4] are the attenuation factors for the incoming and outgoing photons, respectively. For simplicity, we can define a modified mass attenuation factor as

$$\beta(Z' - Z^*) \triangleq \left[\frac{\mu}{\rho}\right]^{in}(Z' - Z_\dagger^*) + \frac{1}{\cos\theta_1}\left[\frac{\mu}{\rho}\right]^{out}(Z' - Z_\dagger^*). \quad [5]$$

Since the collimated photon beam has a finite width, $C_P^{(1)}$ must be integrated over the volume in which scattering takes place, and from which the single-scattered photons reach the detector. Figure 3 shows a ray diagram of the diverging photon beam and the scattering volume that contains point P. Thus, the detector counting rate due to single scattering from the scattering volume is given by

$$C_V^{(1)}(Z_\dagger^*, Z_{min}^*, Z_{max}^*) = \int_{Z_{min}^*}^{Z_{max}^*} \int_{X_{min}(Z_P^*)}^{X_{max}(Z_P^*)} \int_{Y_{min}(Z_P^*, X)}^{Y_{max}(Z_P^*, X)} C_P^{(1)}(Z_\dagger^*, Z_P^*)\, dY\, dX\, dZ_P^*. \quad [6]$$

By assumption, the integrand in [6] has no dependence on X or Y. Therefore, the integration with regard to X and Y results in the term $A_{sv}(Z_P^*)$, which is the local cross-sectional area of the

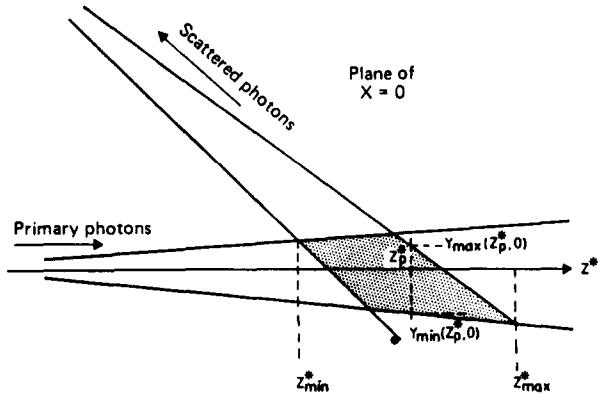

Figure 3. Ray diagram of the scattering volume.

scattering volume. By combining the terms that are determined by the geometry and the characteristics of the densitometer system, we obtain a kernel function

$$K(Z_P^*) \triangleq \epsilon_d \Phi(Z_P^*) \Delta\Omega(Z_P^*) A_{sv}(Z_P^*). \quad [7]$$

Next, we can combine the terms that are material properties:

$$R(Z_P^* - Z_\dagger^*) \triangleq \frac{d\sigma_c}{d\Omega}(Z_P^* - Z_\dagger^*) \rho(Z_P^* - Z_\dagger^*) \exp\left[- \int_{Z_\dagger^*}^{Z_P^*} \rho(Z' - Z_\dagger^*) \beta(Z' - Z_\dagger^*) \, dZ' \right]. \quad [8]$$

Since $K(Z_P^*) = 0$ for $Z_P^* \leqslant Z_{min}^*$ and $Z_P^* \geqslant Z_{max}^*$, and, because of the assumption made earlier that there is no scattering or absorption in the air, $\rho(Z_P^* - Z_\dagger^*) = 0$ for $Z_P^* \leqslant Z_\dagger^*$. Thus, the lower limit of integration in [6], Z_{min}^*, can be set to the position of the surface of the test section, $Z_\dagger^*$. It is convenient to redefine the variables and the functions as follows:

$$Z \triangleq Z_{max}^* - Z_\dagger^*,$$

$$z \triangleq Z_P^* - Z_\dagger^*,$$

$$C^{(1)}(Z) \triangleq C_v^{(1)}(Z_{max}^* - Z, Z_{max}^*),$$

$$K(Z - z) \triangleq K[Z_{max}^* - (Z - z)]$$

and

$$R(z) \triangleq R(Z_P^* - Z_\dagger^*). \quad [9]$$

Combining [7]–[9], [6] yields the following integral:

$$C^{(1)}(Z) = \int_0^Z K(Z - z) R(z) \, dz. \quad [10]$$

Equation [10] is a convolution integral for the counting rate response from single-scattered photons as a function of the distance from the surface of the test section to the upper limit of the scattering volume.

An analysis of multiple-scattered photons indicates (Ohkawa & Lahey 1983) that there are two types of photons; single/multiple-scattered photons, which are scattered once inside the test section but undergo multiple collisions outside the test section, and multiple/multiple-scattered photons, which may undergo multiple scattering both inside and outside the test section. It was found (Ohkawa & Lahey 1983) that the latter can be either neglected or evaluated from the calibration data, and that the former can be modeled in the same way as the single-scattered photons. Thus,

$$C^{(1,m)}(Z) = \int_0^Z K^{(m)}(Z - z) R^{(m)}(z) \, dz, \quad [11]$$

where

$C^{1,m)}(Z)$ = single/multiple-scattering rate,
$K^{(m)}(z)$ = kernel function for multiple scattering

and

$R^{(m)}(Z) = R$ function of the scattering material for multiple scattering.

Therefore, the detector response, [3], can be expressed in more detailed form:

$$D(Z) = \int_0^Z K(Z-z)R(z)\,dz + \int_0^Z K^{(m)}(Z-z)R^{(m)}(z)\,dz + C^{(m,m)}(Z) + B + e(z), \quad [12]$$

where $C^{(m,m)}(Z)$ is the term that quantifies the photons that undergo multiple scattering within the test section. As mentioned previously, it was found (Ohkawa & Lahey 1983) that this term can be combined with the background term, B.

DETERMINATION OF THE KERNEL AND CALIBRATION EXPERIMENT

To calculate the density profile, we must first determine the kernel from data taken for a known density field. Calibration experiments were performed with an annular test section which consisted of a 10.16 cm o.d., 3.81 cm i.d. Lucite pipe and a 1.27 cm dia stainless steel rod. Measurements were taken with the test section, first filled with air, and then filled with water, at 25 locations along the length of photon beam. More than 10,000 counts were taken for each measurement point to obtain a statistical error of $<1\%$. For a 10 Ci ^{137}Cs photon source, a counting time of 700–4000 s per measurement point was required. Hence, the detector responses for the all air, $D_G(Z)$, and all liquid, $D_L(Z)$, cases were obtained. From these data the counting rate due to the multiple-scattered photons could be estimated. The counting rate due to the single-scattered photons was then obtained by subtracting the constant background, B, and the total multiple-scattered photon contribution, $C^{(m)}(Z)$, from $D_G(Z)$. Hence,

$$C_G^{(1)}(Z) = D_G(Z) - [B + C^{(m)}(Z)]. \quad [13]$$

When the scattering volume is the Lucite wall, [12] and [13] imply

$$C_G^{(1)}(Z) = \int_0^Z K(Z-z)R_w(z)\,dz + e_G(Z), \quad [14]$$

where $R_w(z)$ is the R function for the Lucite wall, defined as

$$R_w(z) \triangleq \left[\frac{d\sigma_c}{d\Omega}\right]_w \rho_w \exp(-\rho_w \beta_w z) F_w(z), \quad [15]$$

where

$\left[\frac{d\sigma_c}{d\Omega}\right]_w$ = differential Compton scattering cross section for Lucite, which has the value of 3.776×10^{-3} cm^2/g sr,
$\rho_w = 1.18$ g/cm^3, the density of Lucite,
$\beta_w = 0.2605$ cm^2/g, the attenuation coefficient for Lucite,
$F_w(z)$ = fraction of the cross-sectional area of the photon beam at point z which intercepts the Lucite wall,

$$F_w(z) = \begin{cases} 1.0, & \text{for } 0 \leqslant z \leqslant z_w, \\ 0.0, & \text{for } z_w \leqslant z, \end{cases}$$

z_w = thickness of the Lucite wall, which was, $z_w = 3.175 \pm 0.015$ cm,

and

$e_G(Z)$ = measurement noise, taken to be the statistical counting error.

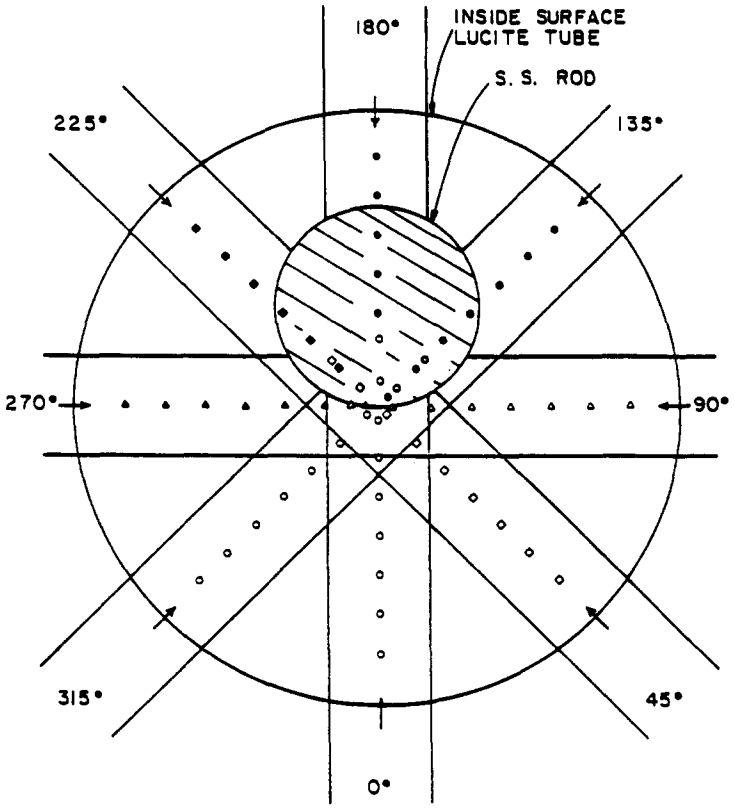

Figure 4. Cross section of an eccentric annulus test section and measurement points.

Since a convolution integral is symmetric, [14] can be rewritten as

$$C_G^{(1)}(Z) = \int_0^Z R_w(Z - z)K(z)\,dz + e_G(Z). \quad [16]$$

Equations [14] and [16] imply that the convolution equation can be solved either as a density function, $R_w(Z)$, or a kernel, $K(z)$, identification problem.

The solution of these integral equations was done numerically. The discretization of [16] was performed by approximating the integration by the trapezoidal rule. The Method of Regularization was used (Ohkawa & Lahey 1983) to evaluate the integral. This technique was previously applied to data taken in a concentric annulus, and good results were reported (Ohkawa & Lahey 1984). In this paper the results of the study of an eccentric annulus are reported.

The local measurement points for the eccentric annulus experiments are shown schematically in figure 4, and typical counting rate and density profiles are shown in figures 5–8. It can be seen that the mixture density is much lower in the wide gap than the narrow gap. Indeed the observed lateral phase distribution is pronounced.

Typical 3-D void profiles are shown in figures 9–13 for the eccentric annulus. It can be seen that in adiabatic air/water experiments of Ohkawa & Lahey (1983) the local void fraction was significantly higher in the wide gap than in the narrow gap. Indeed, for a global void fraction of 80%, run HH, bubbly flow was noted in the narrow gap and annular flow in the wide gap. In fact, it appears that one can pass through the entire flow regime map by circumferentially moving around the rod from the wide to the narrow gap. Thus, it appears that substantial lateral phase separation occurs, and that a more general definition of flow regime is needed for complex geometry conduits.

It is significant to note that prior experiments (Shiralkar & Lahey 1972), which were conducted in boiling freon-114 using a hot-wire anemometer, showed essentially the same data trends. That

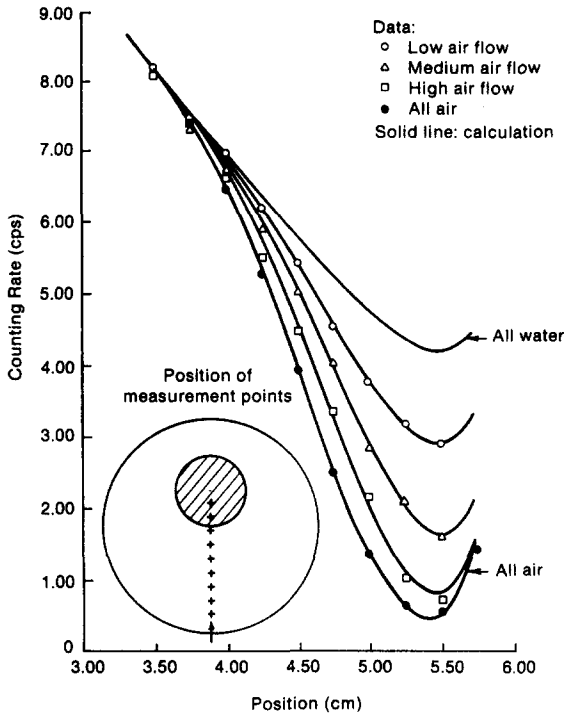

Figure 5. Multiple-scattering-corrected data and predictions based on density solutions for high water flow in the wide gap of an eccentric annulus (0°).

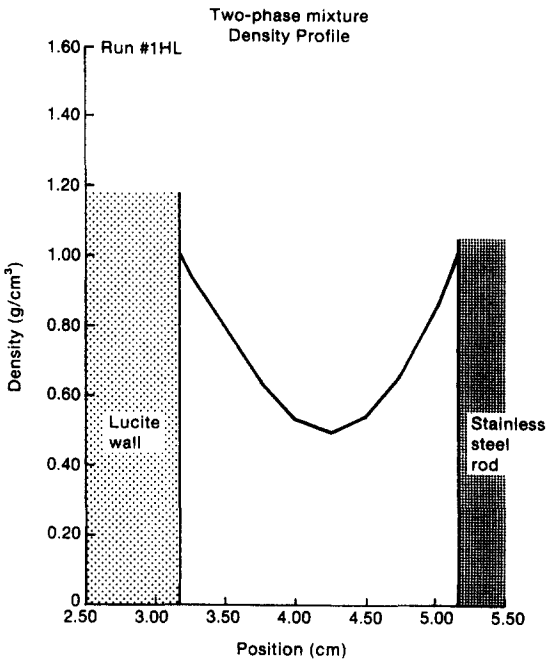

Figure 6. Density profile for high water flow and low air flow; 20% global fraction in the wide gap of an eccentric annulus (0°).

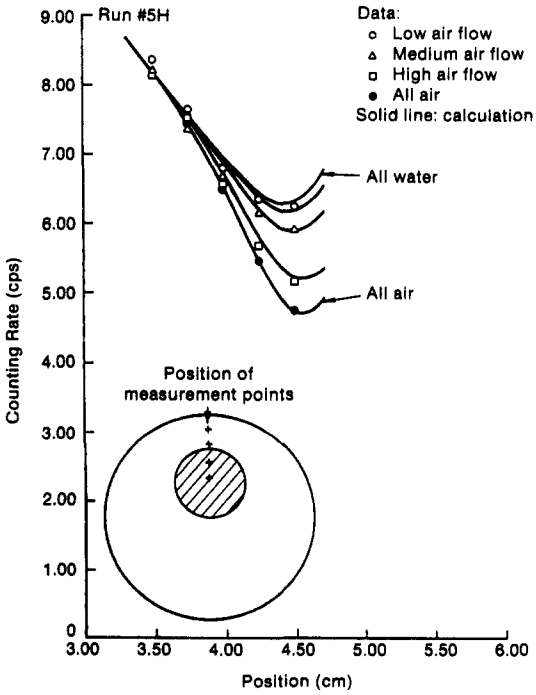

Figure 7. Multiple-scattering-corrected data and predictions based on density solutions for high water flow in the narrow gap of an eccentric annulus (180°).

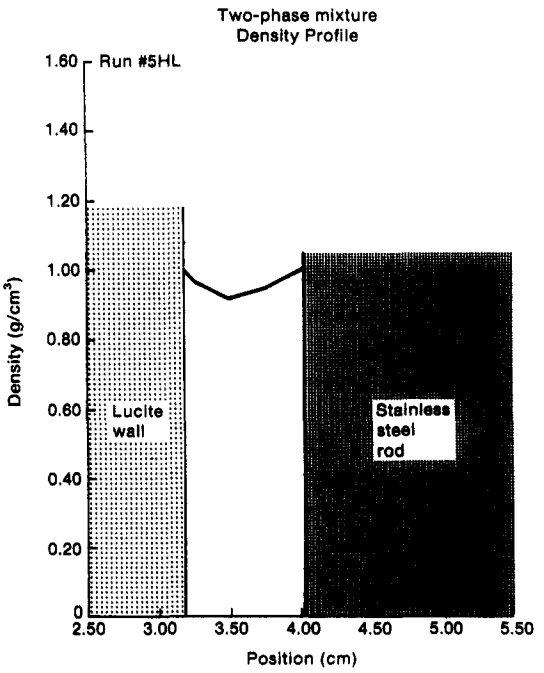

Figure 8. Density profile for high water flow and low air flow; 20% global void fraction in the narrow gap of an eccentric annulus (180°).

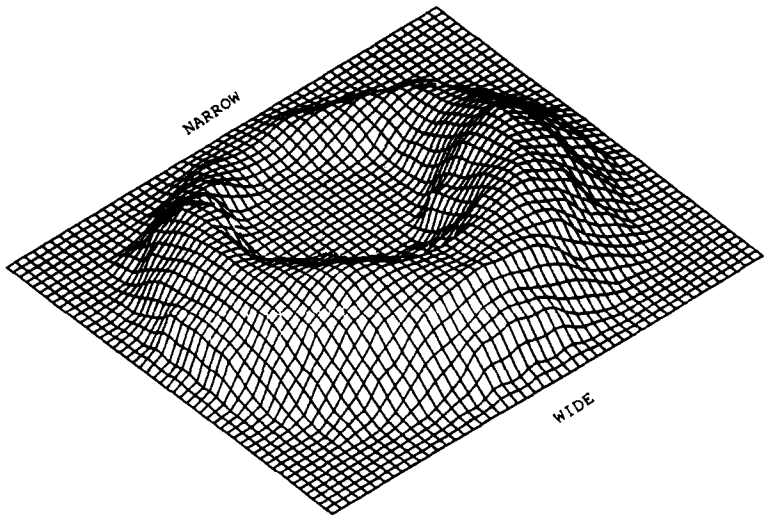

Figure 9. 3-D Map for no water flow and low air flow; 20% global void fraction in an eccentric annulus (run ZL).

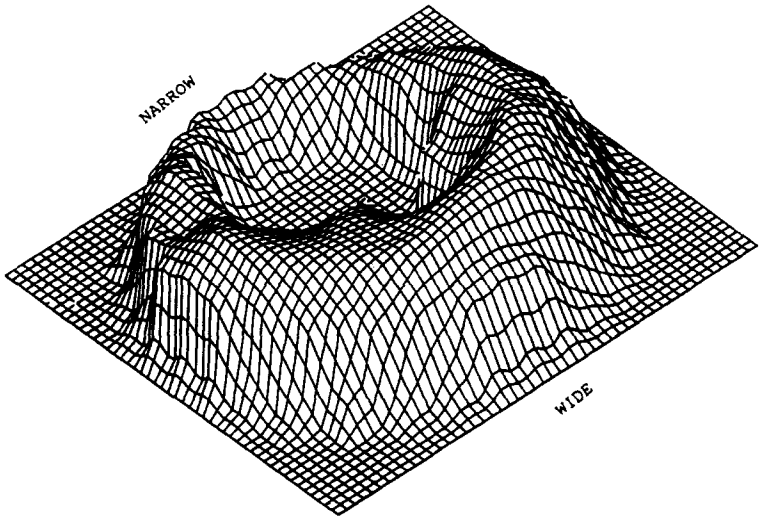

Figure 10. 3-D Map for no water flow and medium air flow; 50% global void fraction in an eccentric annulus (run ZM).

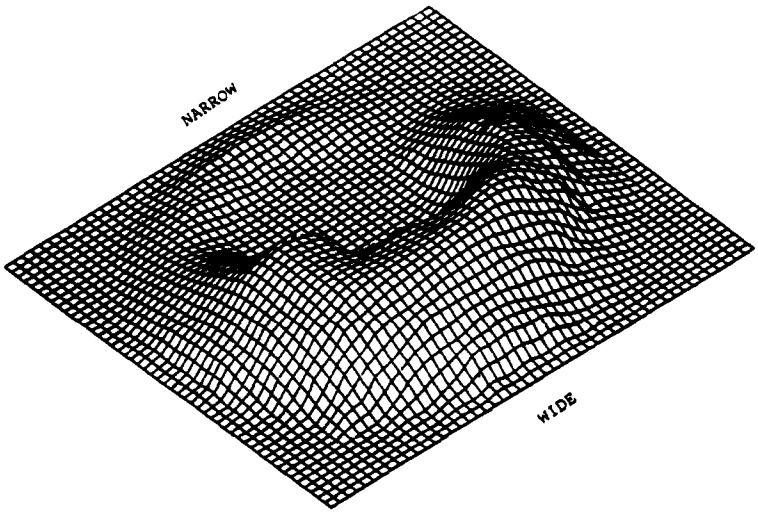

Figure 11. 3-D Map of void fraction for high water flow and low air flow; 20% global void fraction in an eccentric annulus (run HL).

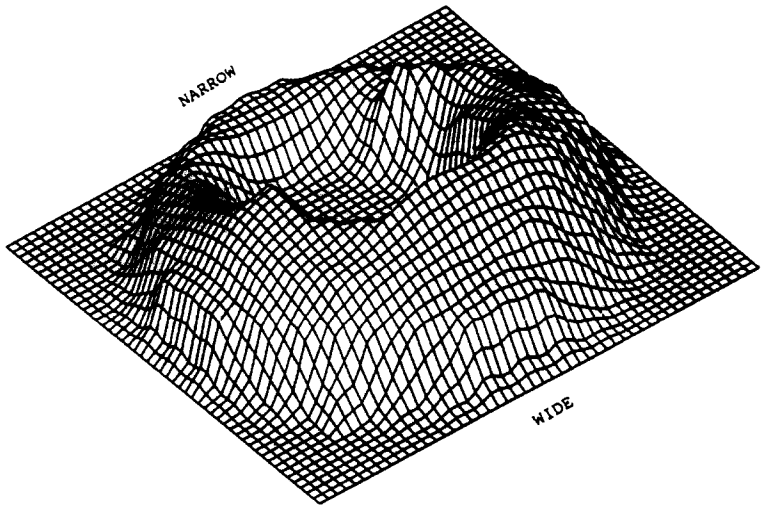

Figure 12. 3-D Map of void fraction for high water flow and medium air flow; 50% global void fraction in an eccentric annulus (run HM).

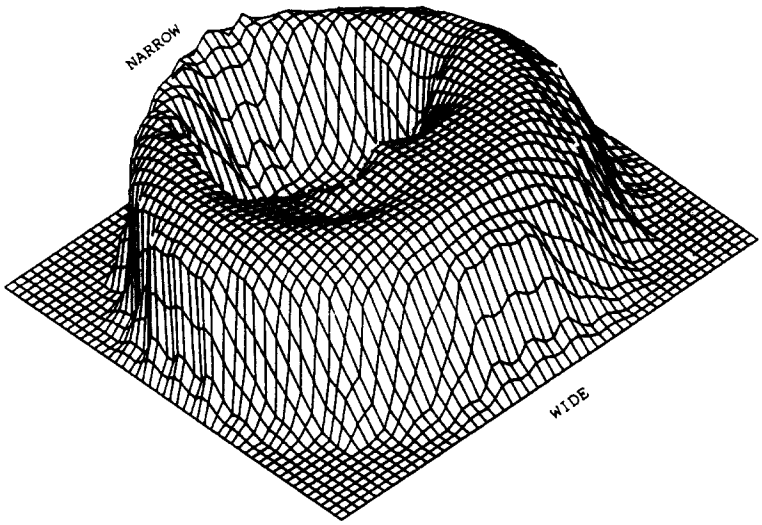

Figure 13. 3-D Map of void fraction for high water flow and high air flow; 80% global void fraction in an eccentric annulus (run HH).

is, the vapor phase always tends to preferentially collect in wide gap regions of an eccentric annulus. Thus, the observed lateral void distribution is apparently not related to the fluids used or the method of vapor formation. Indeed, strong lateral "void drift" forces (Lahey & Moody 1977) are evident.

SUMMARY AND CONCLUSIONS

A thorough understanding of multidimensional phase distribution phenomena is needed before reliable predictions can be made in conduits of complex geometry. The γ-ray scattering densitometer discussed herein allows one to make local void fraction measurements in complex geometry conduits nonintrusively. Indeed, a full set of data have been taken for concentric (Ohkawa & Lahey 1984) and eccentric annuli. Such data are considered vital for model assessment and present a significant challenge to current generation two-fluid models of two-phase flow.

REFERENCES

ELIAS, E. & BEN-HAIM, Y. 1980 Determination of spatial distribution in two-phase flow using scattered gamma radiation. *Nucl. Engng Des.* **59,** 433–441.

KNOLL, G. F. 1979 *Radiation Detection and Measurements.* Wiley, New York.

KONDIC, N. N. & HAHN, O. J. 1970 Theory and application of the parallel and diverging radiation beam method in two-phase systems. *Proc. 4th Int. Conf. Heat Transfer* **7,** 1.5-1–1.5-10.

KONDIC, N. N., JACOBS, A. & EBERT, D. 1983 Three-dimensional density field determination by external stationary detectors and gamma sources using selective scattering. In *ANS Proc. 2nd Int. top. Mtg Nuclear Reactor Thermal Hydraulics*, Santa Barbara, Calif., Vol. 2, pp. 1443–1455.

LAHEY, R. T. JR & MOODY, F. J. 1977 The thermal-hydraulics of a boiling water nuclear reactor. *ANS Monograph.*

OHKAWA, K. & LAHEY, R. T. JR 1983 The development of a gamma-ray scattering densitometer and its application to the measurement of two-phase density distribution in an annular test section. Report NUREG/CR-3374.

OHKAWA, K. & LAHEY, R. T. JR 1984 The development of a gamma-ray scattering densitometer for the nonintrusive measurement of local void fraction. *Nucl. Technol.* **67,** 437–451.

SHIRALKAR, B. S. & LAHEY, R. T. JR 1972 Diabatic local void fraction measurements in freon-114 with a hot wire anemometer. *Trans. Am. nucl. Soc.* **15,** 880.

WANG, S. K., LEE, S. J., JONES, O. C. JR & LAHEY, R. T. JR 1987 Three-dimensional turbulence structure and phase distribution measurements in bubbly two-phase flows. *Int. J. Multiphase Flow* **13,** 327–343.

ZIELKA, L. A. & MACKINNON, J. 1977 Void fraction by gamma scattering. EPRI Project No. RP-765, Electric Power Research Institute, Palo Alto, Calif.